Electronic Supplementary Material (ESI) for Physical Chemistry Chemical Physics.

Supporting information for Photodetachment band of fluorenyl anion: A theoretical rationalization

Abhishek Kumar[1,2], Preeti Karmakar[1], Rudraditya Sarkar*[3], and Tammineni Rajagopala Rao*[1]

[1] *Department of Chemistry, Indian Institute of Technology, Patna, Bihta, Bihar, 801103, India*

[2] *School of Chemical Sciences, Indian Association for the Cultivation of Science, Jadavpur, Kolkata – 700032, India*

[3] *Institut de Química Computacional i Catàlisi (IQCC), Universitat de Girona, 17003 Girona, Catalonia, Spain**

* *rudra.smgr@gmail.com; *rajgopal@iitp.ac.in

I. THEORETICAL METHODOLOGY

A. Computational Details

The electronic ground state of fluorenyl anion (reference geometry) and fluorenyl radical were optimised using the Moller-Plesset perturbation (MP2) level of theory in conjunction with Dunning's cc-pVTZ basis set[1] employing Gaussian 16 program module[2]. The harmonic frequencies of these geometries were also calculated employing the same level of theory and basis set. It is noted that the non availability of the imaginary frequency in the above mentioned Hessian calculations confirmed the energy minimum of the ground state of both fluorenyl anion and fluorenyl radical. The geometry parameters of the energy minimum structure of fluorenyl anion and fluorenyl radical are given in Table S1, while the frequencies of the vibrational modes with a_1 and b_2 symmetry are shown in Table S2 and the frequency of the other vibrational modes are shown in Table S3. The vertical detachment energies (VDEs) at the reference geometry were calculated employing complete active space self-consistent field (CASSCF), CAS second order perturbation theory (CASPT2)[3–5], multi-reference configuration interactions (MRCI) and outer valence green's function (OVGF) level of theories with cc-pVTZ basis set. The outcomes of present calculations are compared with previous experimental[6,7] and theoretical results[7] and the comparative data of VDEs are given in Table I in the main manuscript. The molpro program modules[8] is used to perform calculations at the CASSCF, CASPT2 and MRCI level of theories, whereas the Gaussian16 program modules[2] is used to perform calculations at the OVGF level of theories. The different sets of active spaces; (10,11), (10,12), (12,10), (12,11), (12,12), (14,10), (14,11), (14,11),(14,13), were considered in order to find the best combinations of electrons and molecular orbitals (MOs), such that one can perform computationally feasible and more accurate for CASPT2 and MRCI calculations. According to the current calculations, (10,11) active space, which consists of five valence occupied MOs and six virtual MOs with ten electrons, provides the best comparison with the available experimental value (cf. Table I in the main manuscript). We also notice that the VDE calculated at the OVGF level of theory (cf. Table I in the main manuscript) for the reference geometry of the fluorenyl is closest to the experimental finding[7]. Therefore we have selected the OVGF method for further calculations. It is also found from the previous dynamical study of PAHs[9–11] that the

OVGF method is quite suited for the electronic structure calculations. Later, the reference geometry of the fluorenyl anion was distorted along the dimensionless normal coordinates (DNCs), Q_i (i= 1-41) = $\pm$0.10,$\pm$0.25,. . . .,$\pm$5.00) to generate the single point VDEs.

In order to simulate the photodetachment band of fluorenyl anion using *FC_Class*[12–16] algorithm, we performed optimization followed by frequency calculation of the reference geometry, the electronic ground state of fluorenyl radical, and the first excited state of fluorenyl radical implementing the density functional theory (DFT) and time-dependent-DFT level of theory using 6-311+G* basis sets. These calculations follow the pre-screening of the *FC_Class* simulations[12–16] as given in the Gaussian 16 program module[2]. According to the study mentioned above, the optimized geometries of the reference anion, fluorenyl radical's ground state, and its first excited state belong to C_{2v} point group symmetry. A symbolic picture of the optimized geometries of reference anion with atom number is shown in Fig. S1.

B. Construction of Molecular Hamiltonian

The present study deals with the nuclear dynamics of the first four low-lying electronic states of the fluorenyl radical. These electronic states have following symmetry: $\widetilde{X}^2B_1$, $\widetilde{A}^2A_2$, $\widetilde{B}^2A_2$ and $\widetilde{C}^2B_1$. The states of fluorenyl radical are decided on the basis of the increasing order of VDEs at the reference geometry obtained from different electronic structure calculations. The fluorenyl anion possesses sixty normal modes of vibration, which are decomposed in the following irreducible representation (IREPs):

$$\Gamma = 21a_1 \oplus 10b_1 \oplus 20b_2 \oplus 9a_2. \tag{1}$$

The molecular Hamiltonian is constructed following diabatic electronic representation as described by Köppel *et al*[17,18]. The Hamiltonians are expressed in terms of DNCs (Q) of the vibrational modes. The general form of the constructed Hamiltonian pertinent to the $\widetilde{X}^2B_1$-$\widetilde{A}^2A_2$,-$\widetilde{B}^2A_2$-$\widetilde{C}^2B_1$ electronic states of fluorenyl radical is given by[18]

$$\mathcal{H} = \mathcal{H}_0\mathbf{1} + \mathbf{\Delta}\mathcal{H}, \tag{2}$$

where, $\mathcal{H}$, $\mathcal{H}_0$ and $\Delta\mathcal{H}$ describes overall molecular Hamiltonian, Hamiltonian of reference configuration (unperturbed) and Hamiltonian after the electron detachment, respectively.

1 denotes a unit matrix, whose dimension is equal to the number of considered electronic states, it is a 4×4 unit matrix in the present study. The Hamiltonian of the reference state can be written as[17]:

$$\mathcal{H}_0 = -\frac{1}{2}\sum_{i=a_1,b_1,b_2,a_2}\omega_i\left(\frac{\partial^2}{\partial Q_i^2}\right) + \frac{1}{2}\sum_{i=a_1,b_1,b_2,a_2}\omega_i Q_i^2, \tag{3}$$

where, ω and Q denote the frequency of the normal mode and corresponding DNC at the reference geometry respectively. The standard vibronic selection rules[18–23] are applied to determine the non-vanishing elements of the perturbed Hamiltonian, $\Delta\mathcal{H}$ and it can be written as below:

$$\Delta\mathcal{H} = \begin{pmatrix} E_0^{\widetilde{X}} + \mathcal{U}^{\widetilde{X}} & \sum\limits_{i\in b_2}\lambda_i^{(\widetilde{X}-\widetilde{A})}Q_i & \sum\limits_{i\in b_2}\lambda_i^{(\widetilde{X}-\widetilde{B})}Q_i & \sum\limits_{i\in a_1}\lambda_i^{(\widetilde{X}-\widetilde{C})}Q_i \\ & E_0^{\widetilde{A}} + \mathcal{U}^{\widetilde{A}} & \sum\limits_{i\in a_1}\lambda_i^{(\widetilde{A}-\widetilde{B})}Q_i & \sum\limits_{i\in b_2}\lambda_i^{(\widetilde{A}-\widetilde{C})}Q_i \\ & & E_0^{\widetilde{B}} + \mathcal{U}^{\widetilde{B}} & \sum\limits_{i\in b_2}\lambda_i^{(\widetilde{B}-\widetilde{C})}Q_i \\ h.c. & & & E_0^{\widetilde{C}} + \mathcal{U}^{\widetilde{C}} \end{pmatrix} \tag{4}$$

$$\mathcal{U}^j = \sum_{i\in a_1}\kappa_i^{(j)}Q_i + \frac{1}{2}\sum_{i\in a_1,a_2,b_1,b_2}\gamma_i^{(j)}Q_i^2 + ... \tag{5}$$

Where, E_0^j is the VDE of the jth electronic state, $\kappa_i^{(j)}$ (jth electronic state) and λ_i^{j-k} (between jth and kth electronic states) represent the first-order intra-state and inter-state couplings parameter, respectively. Additionally, the higher-order term $\gamma_i^{(j)}$ denotes the second-order intra-state coupling parameters along all modes.

C. Estimation of Hamiltonian parameters

It should be noted that the parameters of the constructed Hamiltonian were estimated on the basis of two-state-one-mode interaction, which resulted in satisfactory potential fits along each mode (correlation coefficient, R, values of $\sim$ 0.98-0.99). Furthermore, as our research focused solely on non-adiabatic effects in the photodetachment bands, we do not account for the inter-mode coupling that incorporates the Duschinsky rotations. The following steps are used to obtain all of the coupling parameters described above:

1. The single point *ab-initio* energies were calculated at each distortion along DNC of all the vibrational modes.

2. The calculated *ab-initio* potentials were then fitted with the analytic mathematical function, which is obtained from the diagonalization of the Hamiltonian shown in Eq. (4).

3. Finally, the parameters of the Hamiltonian were extracted from the above mentioned fits.

The Hamiltonian parameters obtained from the above procedure are given in Tables S4, S5, and S6.

D. Formulation of Quantum Dynamics Calculation

The nuclear dynamics calculations were performed using multi-configuration time-dependent Hartree (MCTDH) algorithm[24,25] as implemented in Heidelberg MCTDH package[26]. For this study, we have solved both TD and TI Schrödinger wave equation. The former is expressed as a sum of products of single-particle functions (SPFs) $\{\varphi_{j_k}{}^{(k)}\}$ in MCTDH formalism[27,28]. The SPFs in mathematical form can be written as follows:

$$\begin{aligned}\Psi(Q_1,...,Q_f,t) &\equiv \Psi(q_1,...,q_p,t) \\ &= \sum_{j_1}^{n_1}\cdots\sum_{j_p}^{n_p} A_{j_1,...,j_p}(t)\prod_{k=1}^{p}\varphi_{j_k}^{(k)}(q_k,t) \\ &= \sum_{J} A_J\Phi_J\end{aligned} \tag{6}$$

In the above equation, the WF for f degrees of freedom is denoted by the symbol $\Psi(Q_1,...,Q_f,t)$ and the wave function (WF) for p combined modes (MCTDH particles) is denoted by symbol $\Psi(q_1,...,q_p,t)$. Afterward, $\Psi(q_1,...,q_p,t)$ is written in term of product of time-dependent MCTDH coefficients ($A_J \equiv A_{j_1,...,j_p}$) and orthonormal TD SPFs. The symbol Φ_J, at the third line of the product of SPFs, is known as the Hartree product. The TI primitive basis functions are used to expand TD SPFs. For the present calculations, the Hermite discrete variable representation (DVR) is used to construct the primitive basis. It is important to note that the selection of the number of SPFs (n_k) is done such that it is always less than the number of primitive functions (N_x) for each MCTDH particle. These equations also keep a proper balance between two limiting cases of time-dependent-Hartree

(TDH) and standard method [i.e. propagating WP on the primitive basis] of WP propagation. In this fashion, MCTDH introduces a proper correlation between the interacting particles in our calculations.

The equation of motion for the nuclear WF given in Eq. 6 is derived by using Dirac-Frenkel variational principle[29,30]. Thus the MCTDH working equations can be written as follows:

$$i\dot{A}_J = \sum_J <\Phi_J|H|\Phi_L> A_L \tag{7}$$

$$i\dot{\varphi}^{(k)} = (1 - P^{(k)})^{-1}(\rho^{(k)})^{-1} <H>^{(k)} \varphi^{(k)} \tag{8}$$

In the above equation the symbol $\rho^{(k)}$, and $<H>^{(k)}$ is used to represent the one-particle density matrix and the matrix of mean-field operators respectively. The MCTDH projector is denoted by the symbol $P^{(k)}$ which enables SPFs to remain orthonormal during propagation. The propagation of The MCTDH coefficient (A vector) and SPFs (φ vector) are performed by applying a constant mean-field integration scheme (CMF). For this integration, the most efficient short iterative Lancozs (SIL) and Bulirsch-Stoer (BS) integrator for A and φ vectors respectively with variable step sizes are used. An initial WP is constructed such that an electron is removed from the reference ground state of the fluorenyl anion vertically to form four low-lying electronic states of the fluorenyl radical. Afterward, this WP is propagated up to 200 fs in the coupled $\widetilde{X}^2B_1$-$\widetilde{A}^2A_2$-$\widetilde{B}^2A_2$-$\widetilde{C}^2B_1$ electronic states of fluorenyl radical. During this propagation of the WP, the auto-correlation functions [$C(t) = <\Psi(0)|\Psi(t)>$] are recorded. Finally, the autocorrelation functions obtained from discrete calculations are equally weighted and damped with an exponential function ($\exp(\frac{-t}{\tau_r})$). Fourier transform of the obtained autocorrelation function gives an energy value spectrum.

We solved the TI Schrödinger by diagonalizing the Hermitian Hamiltonian given in Eq. (2) using Lanczos algorithm[19,31] as discussed in MCTDH program module[26]. The Hamiltonian of Eq.(2) is represented in the direct product harmonic oscillator (HO) basis of the reference state. The energy eigenvalue obtained in these calculations is convoluted with the Gaussian type of function to get the spectrum envelope.

We have also performed the studies of the nuclear dynamics using block improved relaxation method[27,32,33] to get the eigen energies and the WP densities of the first fifty eigen states. In these calculations, the WP is propagated in negative imaginary time to obtain the information on the ground vibronic state and the A-vector is calculated by diagonalization instead of relaxation. The constant mean-field (CMF) integration scheme applied in these calculations is somewhat different as compared to propagation. Instead of the standard variant of the CMF step size control, CMF/varphi (variable step size), where the CMF step size is controlled only by SPFs, is used in block-improved relaxation calculations as the A-vector changes discontinuously. The determination of the A-vector is performed by using the Davidson diagonalizer. The details of SPFs and HO basis functions used in these studies are presented in Table S8.

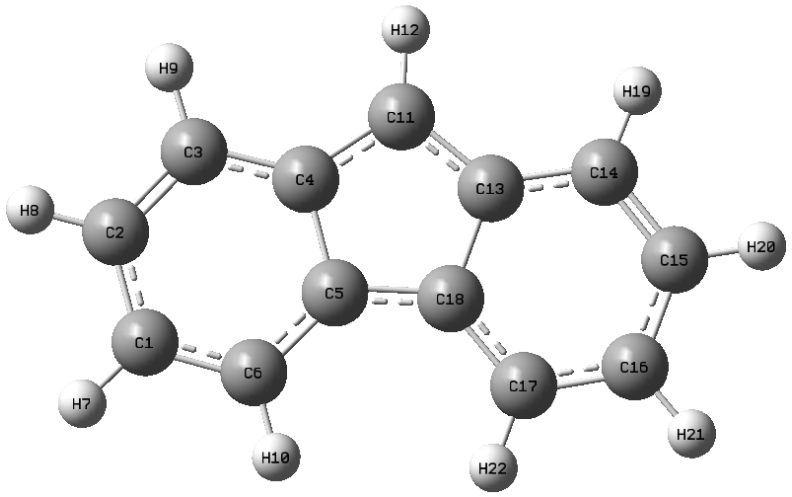

FIG. S1: The schematic numbering of the atoms of the optimized geometry of the fluorenyl anion and neutral fluorenyl radical is presented in this figure to make easier the understanding of the nomenclature of the bonds and bond angles in Table S1.

TABLE S1: Equilibrium ground state geometry parameters of fluorenyl anion and fluorenyl radical with available literature data. The atom numbering is shown in Fig.S1 .

	Theory			
Geometry	Anion		Neutral	
	MP2/cc-pVTZ	B3LYP/6-311+G*	MP2/cc-pVTZ	B3LYP/6-311+G*
$C_{14} - H_{19}$	1.089	1.085	1.086	1.082
$C_{15} - H_{20}$	1.089	1.085	1.085	1.081
$C_{16} - H_{21}$	1.088	1.083	1.085	1.081
$C_{17} - H_{22}$	1.090	1.086	1.086	1.082
$C_{11} - H_{12}$	1.082	1.085	1.083	1.078
$\angle C_{13}C_{14}H_{19}$	120.0	120.07	120.6	120.67
$\angle C_{14}C_{15}H_{20}$	119.5	119.52	119.8	119.79
$\angle C_{15}C_{16}H_{21}$	119.9	119.69	119.6	119.41
$\angle C_{16}C_{17}H_{22}$	119.7	120.07	119.9	120.19
$C_{14} - C_{15}$	1.386	1.386	1.394	1.371
$C_{15} - C_{16}$	1.415	1.415	1.400	1.373
$C_{16} - C_{17}$	1.393	1.388	1.402	1.374
$C_{17} - C_{18}$	1.400	1.402	1.400	1.369
$C_{18} - C_5$	1.438	1.424	1.468	1.422
$C_{18} - C_{13}$	1.53	1.453	1.432	1.407
$C_{13} - C_{11}$	1.415	1.412	1.430	1.439
$C_{13} - C_{14}$	1.417	1.412	1.402	1.469
$\angle C_{13}C_{14}C_{15}$	120.2	120.2	119.0	118.97
$\angle C_{14}C_{15}C_{16}$	121.3	121.69	120.7	120.66
$\angle C_{15}C_{16}C_{17}$	119.8	120.2	120.9	120.12
$\angle C_{16}C_{17}C_{18}$	120.3	119.89	119.1	119.03
$\angle C_{17}C_{18}C_{13}$	120.2	120.38	120.3	119.69
$\angle C_{18}C_{13}C_{14}$	118.3	118.2	120.1	120.53
$\angle C_{13}C_{18}C_5$	107.0	107.08	107.3	108.50
$\angle C_{13}C_{11}C_4$	107.9	107.63	108.4	107.06

TABLE S2: Harmonic frequencies [in cm^{-1} (eV)] of the a_1 and b_2 symmetric vibrational modes of ground state equilibrium structures of fluorenyl anion and fluorenyl radical at MP2/cc-pVTZ level of theory.

Vibrational Mode (Symmetry)	Anion Frequency(ω_i)	Neutral Frequency(ω_i)
$\nu_1(a_1)$	210.60 (0.0261)	221.86 (0.0275)
$\nu_2(a_1)$	430.39 (0.0534)	447.72 (0.0555)
$\nu_3(a_1)$	636.71 (0.0789)	665.82 (0.0825)
$\nu_4(a_1)$	736.98 (0.0914)	808.80 (0.1003)
$\nu_5(a_1)$	876.39 (0.1087)	902.41 (0.1118)
$\nu_6(a_1)$	1020.52 (0.1265)	1102.91 (0.1367)
$\nu_7(a_1)$	1108.25 (0.1374)	1144.31 (0.1419)
$\nu_8(a_1)$	1150.79 (0.1427)	1178.49 (0.1461)
$\nu_9(a_1)$	1220.05 (0.1513)	1211.79 (0.1503)
$\nu_{10}(a_1)$	1321.36 (0.1638)	1280.53 (0.1588)
$\nu_{11}(a_1)$	1347.56 (0.1671)	1332.64 (0.1652)
$\nu_{12}(a_1)$	1399.92 (0.1736)	1388.26 (0.1721)
$\nu_{13}(a_1)$	1493.86 (0.1852)	1526.18 (0.1892)
$\nu_{14}(a_1)$	1551.92 (0.1924)	1571.21 (0.1948)
$\nu_{15}(a_1)$	1598.28 (0.1982)	1754.10 (0.2175)
$\nu_{16}(a_1)$	1651.84 (0.2048)	1816.80 (0.2253)
$\nu_{17}(a_1)$	3152.08 (0.3908)	3216.91 (0.3989)
$\nu_{18}(a_1)$	3160.51 (0.3919)	3224.92 (0.3998)
$\nu_{19}(a_1)$	3176.44 (0.3938)	3237.32 (0.4014)
$\nu_{20}(a_1)$	3197.51 (0.3964)	3250.86 (0.4031)
$\nu_{21}(a_1)$	3215.37 (0.3987)	3273.95 (0.4059)
$\nu_{22}(b_2)$	490.05 (0.0608)	398.59 (0.0494)
$\nu_{23}(b_2)$	536.72 (0.0665)	520.66 (0.0646)
$\nu_{24}(b_2)$	612.79 (0.0759)	644.61 (0.0799)
$\nu_{25}(b_2)$	835.55 (0.1036)	717.24 (0.0889)
$\nu_{26}(b_2)$	1000.36 (0.1240)	884.74 (0.1097)
$\nu_{27}(b_2)$	1018.71 (0.1263)	1061.24 (0.1316)
$\nu_{28}(b_2)$	1121.00 (0.1389)	1086.54 (0.1347)
$\nu_{29}(b_2)$	1149.25 (0.1425)	1144.88 (0.1419)
$\nu_{30}(b_2)$	1155.23 (0.1432)	1193.44 (0.1480)
$\nu_{31}(b_2)$	1246.22 (0.1545)	1237.65 (0.1535)
$\nu_{32}(b_2)$	1365.61 (0.1693)	1255.95 (0.1557)
$\nu_{33}(b_2)$	1426.06 (0.1768)	1357.66 (0.1683)
$\nu_{34}(b_2)$	1501.31 (0.1860)	1542.13 (0.1912)
$\nu_{35}(b_2)$	1547.02 (0.1918)	1582.79 (0.1963)
$\nu_{36}(b_2)$	1567.09 (0.1943)	1810.83 (0.2245)
$\nu_{37}(b_2)$	1635.79 (0.2028)	1848.65 (0.2292)
$\nu_{38}(b_2)$	3151.33 (0.3907)	3215.51 (0.3986)
$\nu_{39}(b_2)$	3156.83 (0.3914)	3222.82 (0.3996)
$\nu_{40}(b_2)$	3175.83 (0.3938)	3236.73 (0.4013)
$\nu_{41}(b_2)$	3196.34 (0.3963)	3249.38 (0.4029)

TABLE S3: Harmonic frequencies [in cm^{-1} (eV)] of the vibrational modes (b_1 and a_2 symmetry) of ground state equilibrium structures of anionic and neutral fluorenyl, calculated at MP2 level of theory using cc-PVTZ basis set

Vibrational Mode(symmetry)	Anion Frequency(ω_i)	Neutral Frequency(ω_i)
$\nu_{42}(b_1)$	107.16(0.0133)	117.81(0.0146)
$\nu_{43}(b_1)$	277.99(0.0345)	338.61(0.0419)
$\nu_{44}(b_1)$	415.36(0.0515)	477.11(0.0591)
$\nu_{45}(b_1)$	546.28(0.0677)	580.48(0.0719)
$\nu_{46}(b_1)$	607.93(0.0754)	692.59(0.0858)
$\nu_{47}(b_1)$	638.99(0.0792)	828.89(0.1027)
$\nu_{48}(b_1)$	709.79(0.0880)	873.96(0.1083)
$\nu_{49}(b_1)$	786.58(0.0975)	1016.25(0.1259)
$\nu_{50}(b_1)$	856.50(0.1061)	1097.54(0.1361)
$\nu_{51}(b_1)$	880.61(0.1092)	1125.55(0.1396)
$\nu_{52}(a_2)$	138.88(0.0172)	157.91(0.0195)
$\nu_{53}(a_2)$	287.38(0.0356)	317.31(0.0393)
$\nu_{54}(a_2)$	414.58(0.0514)	503.00(0.0624)
$\nu_{55}(a_2)$	549.82(0.0681)	660.80(0.0819)
$\nu_{56}(a_2)$	651.22(0.0807)	848.66(0.1052)
$\nu_{57}(a_2)$	710.12(0.0881)	901.44(0.1117)
$\nu_{58}(a_2)$	784.38(0.0972)	1017.85(0.1261)
$\nu_{59}(a_2)$	843.03(0.1045)	1096.47(0.1359)
$\nu_{60}(a_2)$	877.35(0.1087)	1123.36(0.1393)

TABLE S4: Linear and quadratic intrastate coupling parameters (in eV) of tuning modes in the $\widetilde{X}^2B_1$, $\widetilde{A}^2A_2$, $\widetilde{B}^2A_2$ and $\widetilde{C}^2B_1$ electronic states of fluorenyl radical. The excitation strengths of these couplings are given in parentheses.

Mode	$\kappa((\kappa^2)/2\omega^2)$	γ	$\kappa((\kappa^2)/2\omega^2)$	γ
	X^2B_1		A^2A_2	
$\nu_1(a_1)$	-0.0086(0.0546)	0.0027	0.0070(0.0361)	-0.0008
$\nu_2(a_1)$	0.0069(0.0083)	-0.0003	0.0628(0.6913)	-0.0009
$\nu_3(a_1)$	0.0449(0.1616)	0.0010	-0.0046(0.0017)	-0.0040
$\nu_4(a_1)$	-0.0265(0.0421)	-0.0009	0.0725(0.3143)	0.0023
$\nu_5(a_1)$	0.0271(0.03115)	0.0004	-0.0511(0.11069)	0.0015
$\nu_6(a_1)$	-0.0025(0.0002)	0.0021	0.0067(0.0014)	0.0022
$\nu_7(a_1)$	-0.0369(0.0362)	0.0035	0.0556(0.0820)	0.0033
$\nu_8(a_1)$	0.0326(0.0263)	0.0067	-0.0533(0.0694)	0.0073
$\nu_9(a_1)$	-0.0182(0.0073)	0.0025	0.0053(0.00062)	0.0012
$\nu_{10}(a_1)$	-0.0112(0.0024)	0.0027	-0.0150(0.0042)	0.0024
$\nu_{11}(a_1)$	-0.0683(0.0836)	-0.0009	0.0564(0.0570)	0.0014)
$\nu_{12}(a_1)$	0.0268(0.01193)	-0.0034)	-0.0517(0.0445)	0.0069
$\nu_{13}(a_1)$	0.0035(0.0002)	0.0032	-0.0274(0.01099)	-0.0004)
$\nu_{14}(a_1)$	0.0849(0.0973)	0.0017	-0.1323(0.2365)	0.0068
$\nu_{15}(a_1)$	-0.1163(0.1723)	0.0026	0.1113(0.1577)	0.0016
$\nu_{16}(a_1)$	-0.0025(0.0000)	-0.0018	0.0665(0.0528)	-0.0171
$\nu_{17}(a_1)$	-0.0033(0.0000)	0.0052	0.0055(0.0001)	0.0056
$\nu_{18}(a_1)$	-0.0117(0.0005)	0.0039	-0.01844(0.0011)	0.0044
$\nu_{19}(a_1)$	0.0106(0.00035)	0.0043	0.0082(0.0002)	0.0043
$\nu_{20}(a_1)$	-0.0221(0.0015)	0.0035)	-0.0291(0.0027)	0.0035
$\nu_{21}(a_1)$	0.0115(0.0004)	0.0054	0.0165(0.0009)	0.0043
	B^2A_2		C^2B_1	
$\nu_1(a_1)$	-0.0011(0.0008)	-0.0034	-0.0001(0.0000)	-0.0031
$\nu_2(a_1)$	-0.0257(0.1159)	-0.0009	-0.0352(0.2178)	-0.0037
$\nu_3(a_1)$	-0.0023(0.0004)	0.0021	-0.0310(0.0769)	-0.0029
$\nu_4(a_1)$	-0.0171(0.0175)	-0.0014	0.0319(0.0609)	-0.0047
$\nu_5(a_1)$	-0.0151(0.0096)	-0.00076	0.01058(0.0047)	0.0003
$\nu_6(a_1)$	0.01319(0.0054)	0.0002	0.01599(0.0079)	-0.0018
$\nu_7(a_1)$	-0.0121(0.0039)	-0.0002	-0.0020(0.0001)	-0.0027
$\nu_8(a_1)$	0.0262(0.0168)	0.0064	0.0328(0.0266)	0.0063
$\nu_9(a_1)$	0.0316(0.0217)	0.0079	-0.0555(0.0676)	-0.0008
$\nu_{10}(a_1)$	0.0131(0.0032)	0.0045	0.0463(0.0399)	-0.0087
$\nu_{11}(a_1)$	0.0589(0.0617)	0.0042	-0.02336(0.0098)	0.0092
$\nu_{12}(a_1)$	0.0232(0.0088)	0.0053	0.0502(0.0418)	-0.0024
$\nu_{13}(a_1)$	-0.0031(0.0002)	-0.0045	0.0639(0.0596)	-0.0137
$\nu_{14}(a_1)$	0.1343(0.2436)	0.0082	0.0446(0.0269)	-0.0049
$\nu_{15}(a_1)$	0.0347(0.0153)	0.0143	0.0236(0.0071)	-0.0037
$\nu_{16}(a_1)$	-0.03234(0.0125)	0.0201	0.0574(0.0393)	0.0071
$\nu_{17}(a_1)$	0.0012(0.0000)	0.0048	0.0036(0.0000)	0.0049
$\nu_{18}(a_1)$	-0.0076(0.0002)	0.0035	-0.0095(0.0003)	0.0035
$\nu_{19}(a_1)$	0.0099(0.0003)	0.0040	0.0116(0.0004)	0.0041
$\nu_{20}(a_1)$	-0.0301(0.0029)	0.0029	-0.0302(0.0029)	0.0031
$\nu_{21}(a_1)$	0.0107(0.0004)	0.0033	0.0118(0.0004)	0.0034

TABLE S5: The quadratic intrastate coupling parameters (in eV) of b_2 coupling modes in the in the $\widetilde{X}^2B_1$, $\tilde{A}^2B_1$, $\widetilde{B}^2A_2$ and $\widetilde{C}^2B_1$ electronic states of fluorenyl radical.

Vibrational modes	X^2B_1	A^2A_2	B^2A_2	C^2B_1
ν_{22}	-0.0015	0.0039	-0.0008	-0.0011
ν_{23}	-0.0012	-0.0002	-0.0030	0.0032
ν_{24}	-0.0008	-0.0012	-0.0097	0.0047
ν_{25}	0.0003	0.0002	-0.0030	0.0033
ν_{26}	0.0002	0.0002	-0.0041	0.0056
ν_{27}	0.0024	0.0023	0.0005	0.0001
ν_{28}	0.0025	0.0051	0.0006	0.0012
ν_{29}	0.0016	0.0120	0.0064	0.0064
ν_{30}	0.0049	0.0056	-0.0009	0.0127
ν_{31}	-0.0004	0.0029	0.0039	0.0115
ν_{32}	-0.0053	0.0088	0.0111	0.0099
ν_{33}	0.0008	0.0085	0.0034	0.0038
ν_{34}	-0.0066	0.0064	0.0058	-0.0018
ν_{35}	-0.0293	0.0373	0.0147	0.0101
ν_{36}	-0.0036	-0.0006	-0.0243	0.0286
ν_{37}	-0.0087	0.0128	-0.0016	0.0119
ν_{38}	0.0051	0.0055	0.0047	0.0047
ν_{39}	0.0044	0.0048	0.0044	0.0036
ν_{40}	0.0044	0.0045	0.0042	0.0041
ν_{41}	0.0038	0.0038	0.0033	0.0033

TABLE S6: The linear interstate coupling parameter (in eV) between the electronic states of fluorenyl radical. The coupling strength ($\lambda_i^2/2\omega_i^2$) of these coupling modes are given in parentheses.

Coupled states	Vib mode (symmetry)	$\lambda((\lambda^2)/2\omega^2)$	Coupled states	Vib mode (symmetry)	$\lambda((\lambda^2)/2\omega^2)$
$\tilde{X}-\tilde{A}$	$\nu_{22}(b_2)$	0.0432(0.2532)	$\tilde{X}-\tilde{B}$	$\nu_{22}(b_2)$	0.0223(0.0670)
	$\nu_{23}(b_2)$	0.0196(0.0435)		$\nu_{23}(b_2)$	0.0335(0.1265)
	$\nu_{24}(b_2)$	0.0108(0.0101)		$\nu_{24}(b_2)$	0.0769(0.5131)
	$\nu_{25}(b_2)$	0.0086(0.0035)		$\nu_{25}(b_2)$	0.0463(0.0996)
	$\nu_{26}(b_2)$	0.0054(0.0009)		$\nu_{26}(b_2)$	0.0523(0.0888)
	$\nu_{27}(b_2)$	0.0062(0.0012)		$\nu_{27}(b_2)$	0.0362(0.0409)
	$\nu_{28}(b_2)$	0.0294(0.0224)		$\nu_{28}(b_2)$	0.0362(0.0341)
	$\nu_{29}(b_2)$	0.0603(0.0895)		$\nu_{29}(b_2)$	0.0577(0.0821)
	$\nu_{30}(b_2)$	0.0157(0.0061)		$\nu_{30}(b_2)$	0.0603(0.0885)
	$\nu_{31}(b_2)$	0.0316(0.0209)		$\nu_{31}(b_2)$	0.0546(0.0625)
	$\nu_{32}(b_2)$	0.0706(0.08705)		$\nu_{32}(b_2)$	0.1068(0.1990)
	$\nu_{33}(b_2)$	0.0517(0.0428)		$\nu_{33}(b_2)$	0.0423(0.0286)
	$\nu_{34}(b_2)$	0.067(0.0664)		$\nu_{34}(b_2)$	0.0932(0.1253)
	$\nu_{35}(b_2)$	0.1519(0.3136)		$\nu_{35}(b_2)$	0.1656(0.3726)
	$\nu_{36}(b_2)$	0.0300(0.0119)		$\nu_{36}(b_2)$	0.1010(0.1352)
	$\nu_{37}(b_2)$	0.0812(0.0802)		$\nu_{37}(b_2)$	0.0841(0.0859)
	$\nu_{38}(b_2)$	0.0125(0.0005)		$\nu_{38}(b_2)$	0.0160(0.0009)
	$\nu_{39}(b_2)$	0.0127(0.0005)		$\nu_{39}(b_2)$	0.0034(0.0000)
	$\nu_{40}(b_2)$	0.0054(0.0000)		$\nu_{40}(b_2)$	0.0108(0.0004)
	$\nu_{41}(b_2)$	0.0023(0.0000)		$\nu_{41}(b_2)$	0.0196(0.0012)
$\tilde{A}-\tilde{C}$	$\nu_{22}(b_2)$	0.0518(0.3645)	$\tilde{B}-\tilde{C}$	$\nu_{22}(b_2)$	0.0072(0.0071)
	$\nu_{23}(b_2)$	0.0425(0.2038)		$\nu_{23}(b_2)$	0.0361(0.1476)
	$\nu_{24}(b_2)$	0.0570(0.2820)		$\nu_{24}(b_2)$	0.0572(0.2835)
	$\nu_{25}(b_2)$	0.0405(0.0764)		$\nu_{25}(b_2)$	0.0357(0.0594)
	$\nu_{26}(b_2)$	0.0536(0.0937)		$\nu_{26}(b_2)$	0.0448(0.0653)
	$\nu_{27}(b_2)$	0.0357(0.0399)		$\nu_{27}(b_2)$	0.0103(0.0034)
	$\nu_{28}(b_2)$	0.0455(0.0535)		$\nu_{28}(b_2)$	0.0119(0.0037)
	$\nu_{29}(b_2)$	0.0548(0.0739)		$\nu_{29}(b_2)$	0.0034(0.0003)
	$\nu_{30}(b_2)$	0.0626(0.0958)		$\nu_{30}(b_2)$	0.0545(0.0725)
	$\nu_{31}(b_2)$	0.0687(0.0988)		$\nu_{31}(b_2)$	0.0389(0.0317)
	$\nu_{32}(b_2)$	0.0199(0.0069)		$\nu_{32}(b_2)$	0.0152(0.0041)
	$\nu_{33}(b_2)$	0.0503(0.0406)		$\nu_{33}(b_2)$	0.0092(0.0014)
	$\nu_{34}(b_2)$	0.0663(0.0635)		$\nu_{34}(b_2)$	0.0388(0.0218)
	$\nu_{35}(b_2)$	0.1081(0.1588)		$\nu_{35}(b_2)$	0.0295(0.01184)
	$\nu_{36}(b_2)$	0.1181(0.1846)		$\nu_{36}(b_2)$	0.1059(0.1486)
	$\nu_{37}(b_2)$	0.0179(0.0039)		$\nu_{37}(b_2)$	0.0490(0.0292)
	$\nu_{38}(b_2)$	0.0211(0.00145)		$\nu_{38}(b_2)$	0.0029(0.0000)
	$\nu_{39}(b_2)$	0.0259(0.0022)		$\nu_{39}(b_2)$	0.0125(0.0005)
	$\nu_{40}(b_2)$	0.0147(0.0007)		$\nu_{40}(b_2)$	0.0052(0.0001)
	$\nu_{41}(b_2)$	0.0168(0.0009)		$\nu_{41}(b_2)$	0.0019(0.0000)

TABLE S7: Estimated energy (in eV) of equilibrium minimum (Diagonal ones) of electronic states and a minimum of CIs (off-diagonal ones) between different electronic states of fluorenyl radical.

	$\widetilde{X}^2B_1$	$\widetilde{A}^2A_2$	$\widetilde{B}^2A_2$	$\widetilde{C}^2B_1$
$\widetilde{X}^2B_1$	1.6332	3.1053	14.4785	21.4413
$\widetilde{A}^2A_2$		2.8648	5.0673	7.8723
$\widetilde{B}^2A_2$			4.3547	6.1477
$\widetilde{C}^2B_1$				5.1809

TABLE S8: Normal modes combination, size of the primitive basis and single particle functions (SPFs) used in the time-dependent and time-independent nuclear dynamics studies within MCTDH framework.

Combination of normal modes	Primitive basis	SPF	Figure
ν_1, ν_6, ν_9, ν_{13}, ν_{20}	2		Fig. 2c (green and blue stick spectra)
ν_2, ν_4, ν_{10}, ν_{14}, ν_{15}	4		
ν_3, ν_5, ν_7, ν_8,ν_{11}, ν_{12}	3		
ν_2, ν_4, ν_{10}, ν_{14}, ν_{15}	14	[10,10]	Fig. 2c (black and red envelope)
ν_3, ν_5, ν_7, ν_8,ν_{11}, ν_{12}	10	[8,8]	
ν_1, ν_6, ν_9, ν_{13}, ν_{20}	9	[6,6]	
ν_2, ν_3, ν_4	4		Fig. 2d (stick spectra)
ν_1, ν_{11}, ν_{23}, ν_{29}, ν_{32}	3		
ν_5, ν_7, ν_8, ν_9, ν_{14}, ν_{15}	2		
ν_2, ν_3, ν_4, ν_{14}, ν_{22}, ν_{35}	14	[10,10]	Fig. 2e, Fig. 2f
ν_7, ν_8, ν_9, ν_{12}	12	[8,8]	
ν_1, ν_5, ν_{11}	11	[7,7]	
ν_{23}, ν_{29}, ν_{32}	10	[6,6]	
ν_3, ν_4, ν_{14}, ν_{15}	14	[10,10]	Fig. 4
ν_5, ν_7, ν_8, ν_{11}, ν_{12}	10	[8,8]	
ν_1, ν_2, ν_{10}	9	[6,6]	
ν_6, ν_9, ν_{13}, ν_{20}	8	[4,4]	
ν_2, ν_4, ν_{14}, ν_{22}, ν_{35}	12	[14,14]	Fig. 5
ν_3, ν_7, ν_8, ν_9, ν_{12}	10	[12,12]	
ν_1, ν_5, ν_{11}	8	[11,11]	
ν_{23}, ν_{29}, ν_{32}	7	[10,10]	
ν_2, ν_4, ν_{14}, ν_{22}, ν_{35}	14	[10,10,10,10]	Fig. S3
ν_3, ν_7, ν_8, ν_9, ν_{12}	12	[8,8,8,8]	
ν_1, ν_5, ν_{11}	11	[7,7,7,7]	
ν_{23}, ν_{29}, ν_{32}	10	[6,6,6,6]	

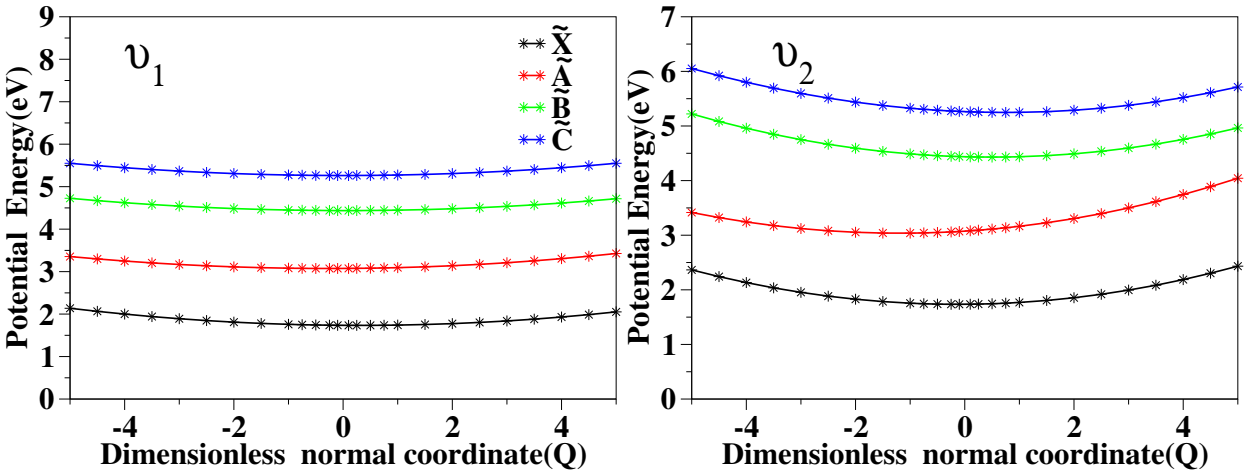
υ1
X̃
Ã
B̃
C̃
Potential Energy(eV)
Dimensionless normal coordinate(Q)

(a)

υ2
Potential Energy(eV)
Dimensionless normal coordinate(Q)

(b)

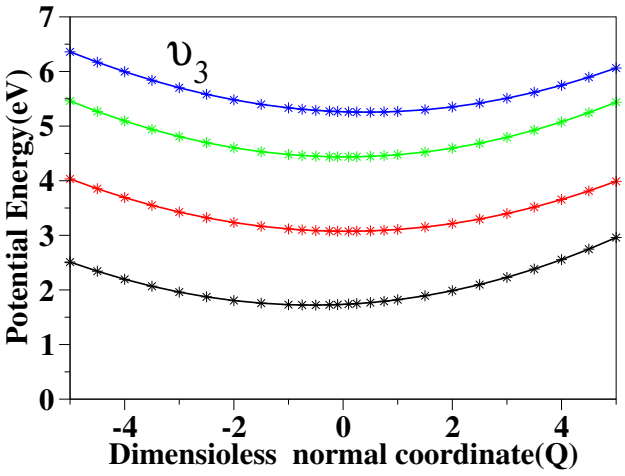
υ3
Potential Energy(eV)
Dimensioless normal coordinate(Q)

(c)

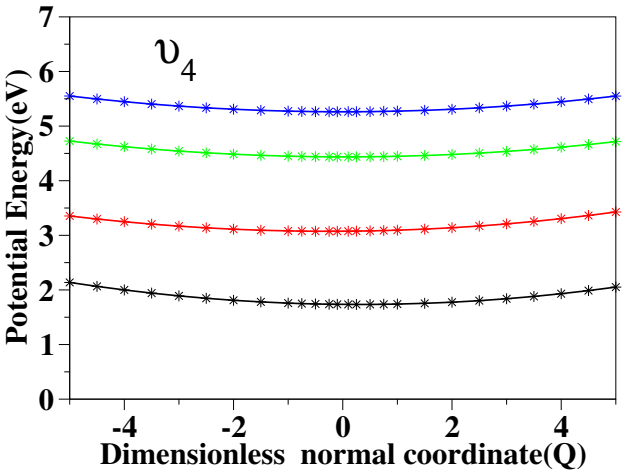
υ4
Potential Energy(eV)
Dimensionless normal coordinate(Q)

(d)

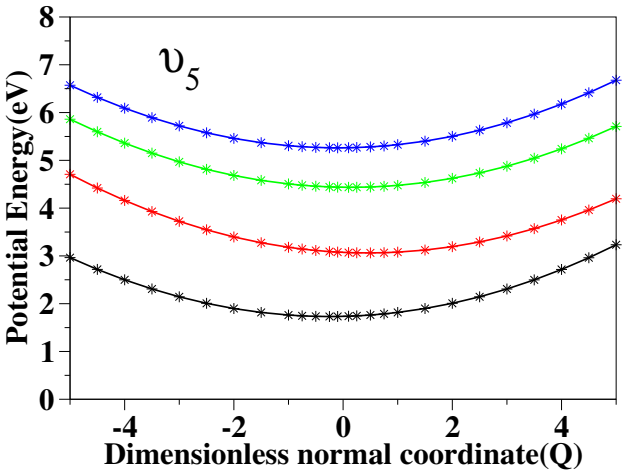
υ5
Potential Energy(eV)
Dimensionless normal coordinate(Q)

(e)

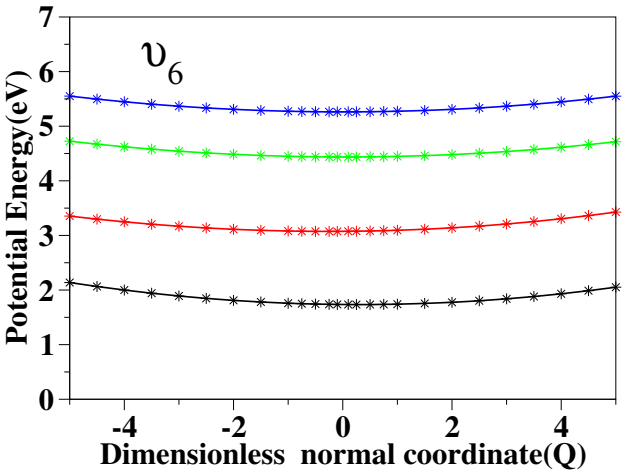
υ6
Potential Energy(eV)
Dimensionless normal coordinate(Q)

(f)

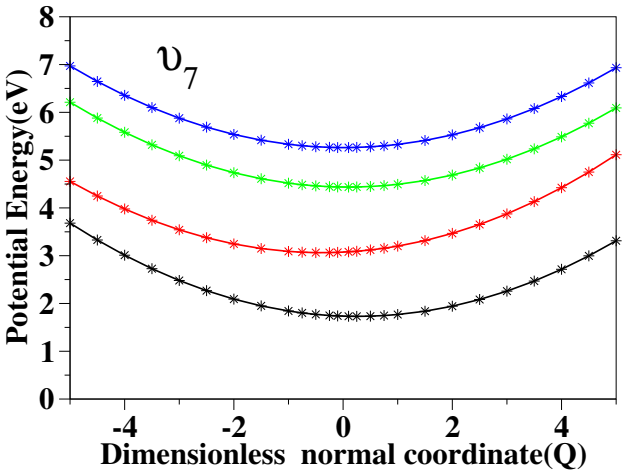
υ7
Potential Energy(eV)
Dimensionless normal coordinate(Q)

(g)

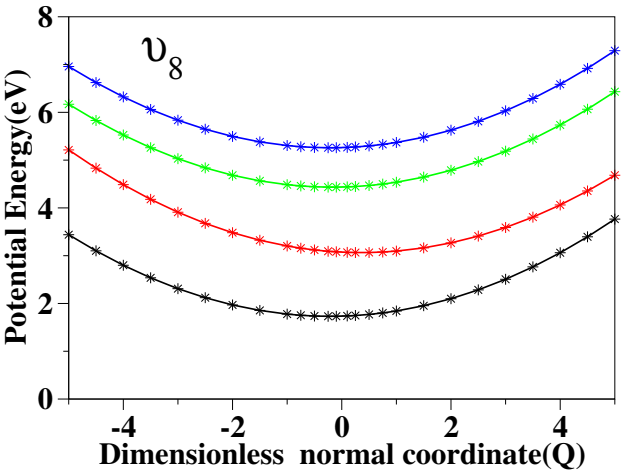
υ8
Potential Energy(eV)
Dimensionless normal coordinate(Q)

(h)

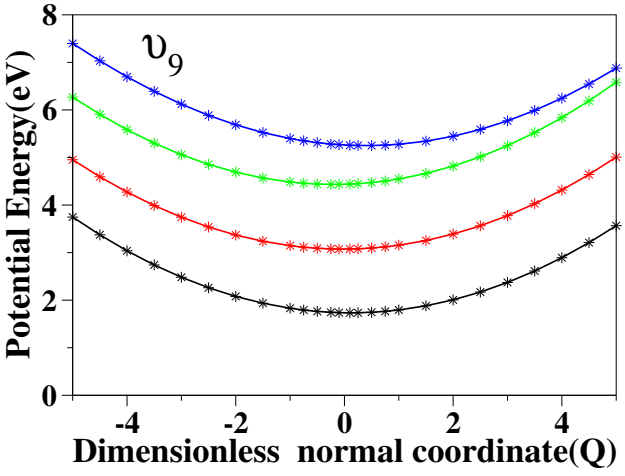
υ9
Potential Energy(eV)
Dimensionless normal coordinate(Q)

(i)

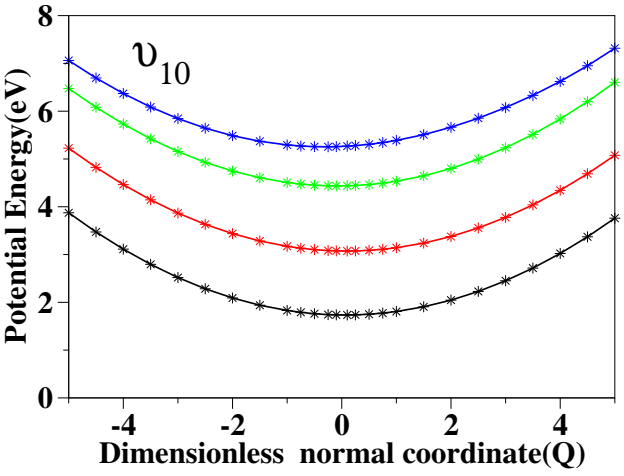
υ10
Potential Energy(eV)
Dimensionless normal coordinate(Q)

(j)

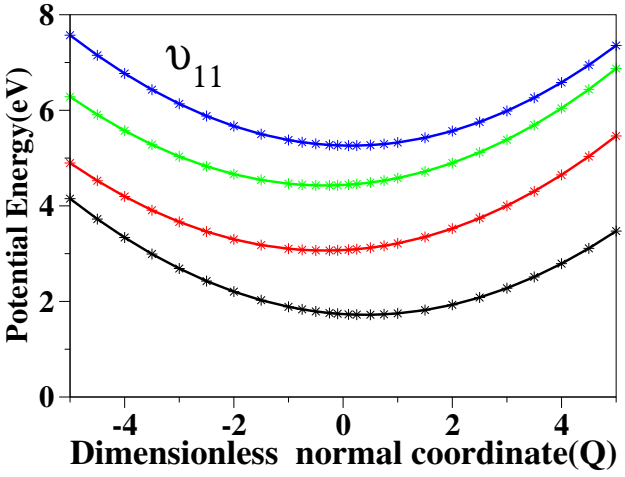
υ11
Potential Energy(eV)
Dimensionless normal coordinate(Q)

(k)

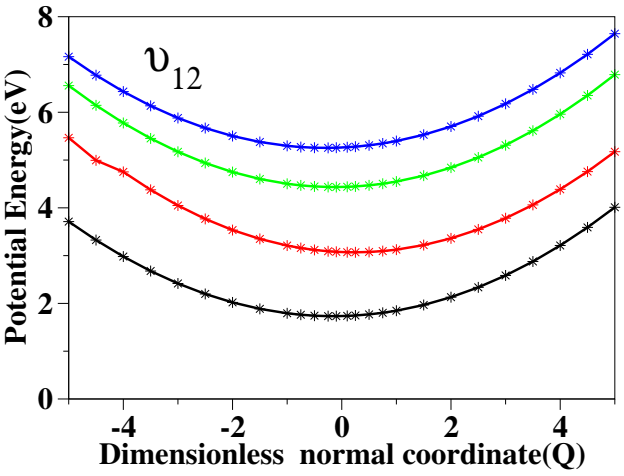
υ12
Potential Energy(eV)
Dimensionless normal coordinate(Q)

(l)

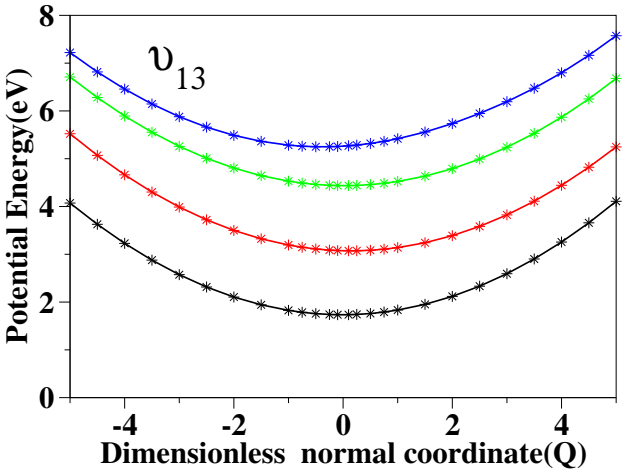
υ13
Potential Energy(eV)
Dimensionless normal coordinate(Q)

(m)

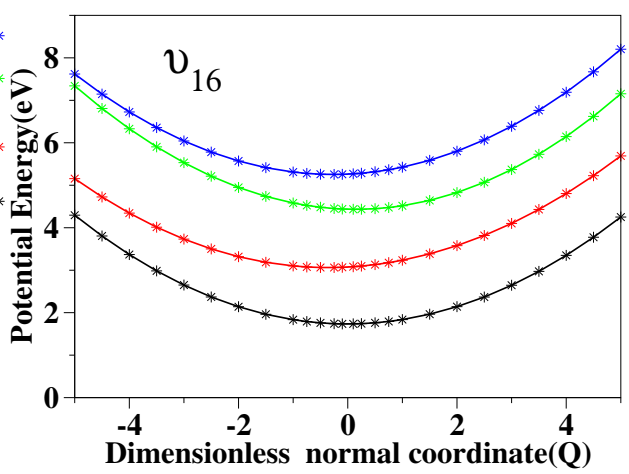
υ16
Potential Energy(eV)
Dimensionless normal coordinate(Q)

(n)

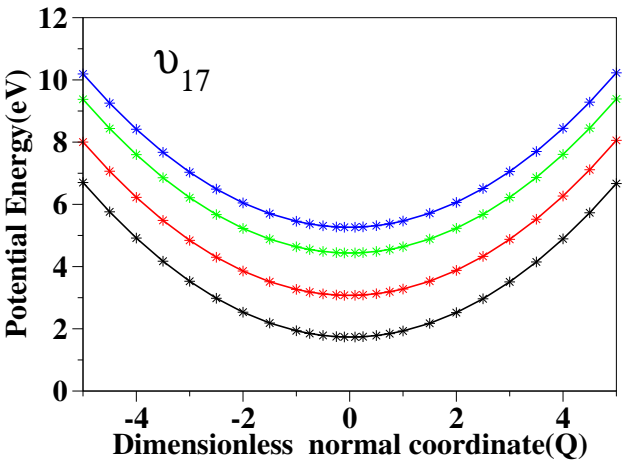
υ17
Potential Energy(eV)
Dimensionless normal coordinate(Q)

(o)

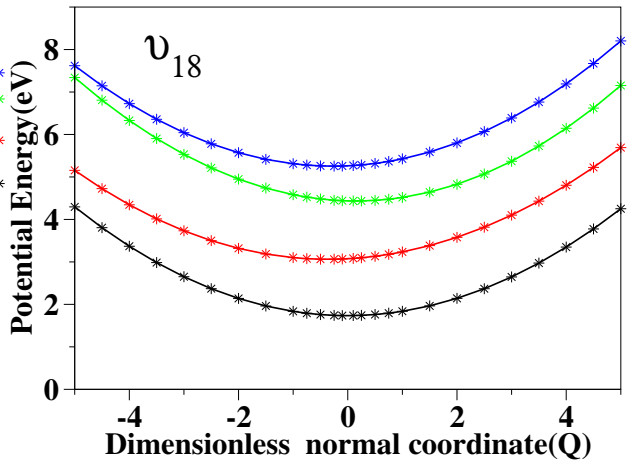
υ18
Potential Energy(eV)
Dimensionless normal coordinate(Q)

(p)

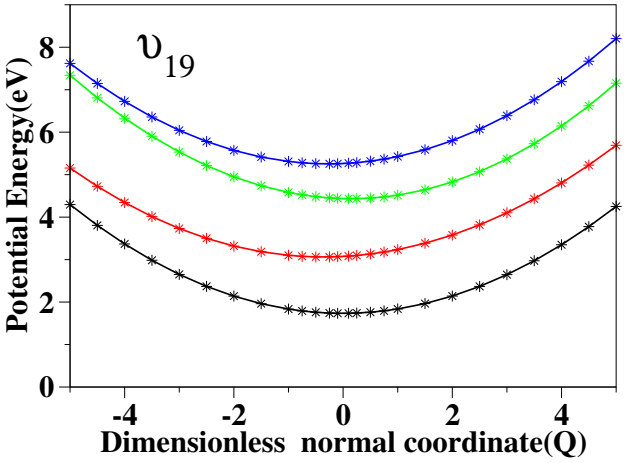
υ19
Potential Energy(eV)
Dimensionless normal coordinate(Q)

(q)

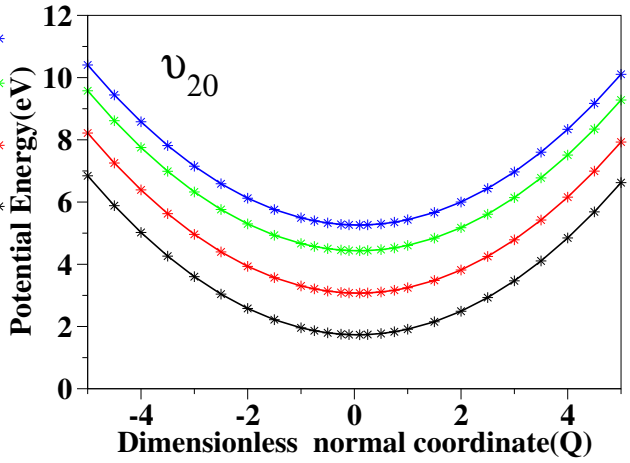
υ20
Potential Energy(eV)
Dimensionless normal coordinate(Q)

(r)

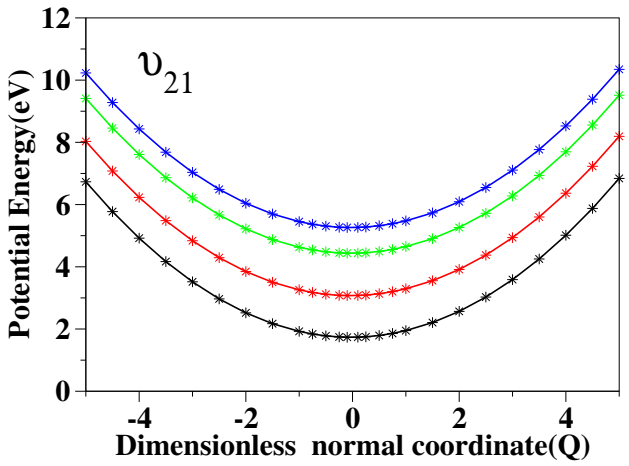

(s)

FIG. S2: One dimensional PECs along dimensionless normal coordinate of all totally symmetric vibrational modes except Q_{14} and Q_{15}.

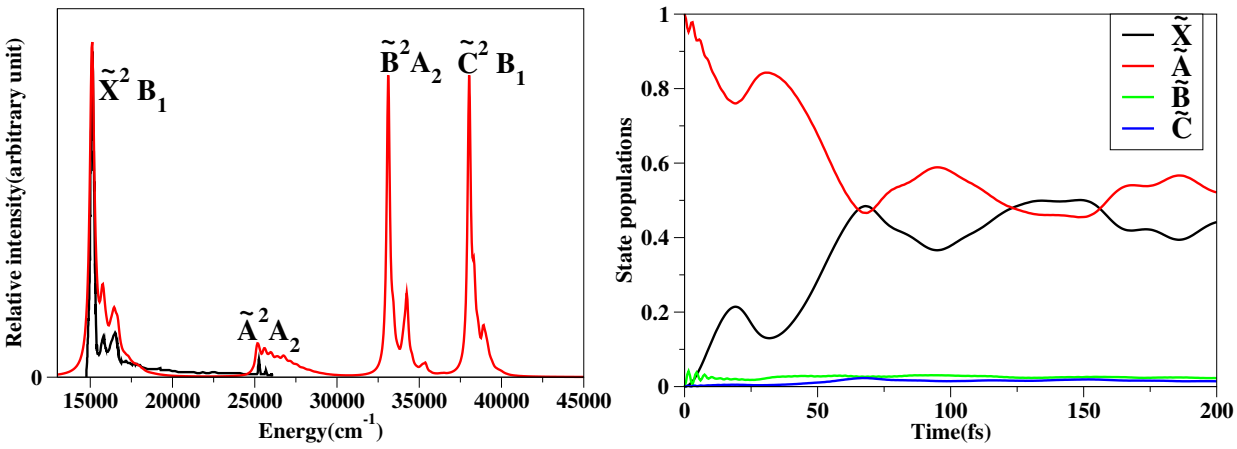

(a) (b)

FIG. S3: The comparison between the experimental SEVI spectra (digitized from reference[7]) and spectra obtained from coupled $\widetilde{X}^2B_1$-$\widetilde{A}^2A_2$-$\widetilde{B}^2A_2$-$\widetilde{C}^2B_1$ states dynamics following time-dependent approach is shown in panel a. The black envelope corresponds to experimental observation and the red envelope is obtained from the present theoretical calculations. The electronic population transfer from $\widetilde{A}^2A_2$ state to $\widetilde{X}^2B_1$, $\widetilde{B}^2A_2$ and $\widetilde{C}^2B_1$ states of fluorenyl radical is shown in panel b when the initial wavepacket is prepared in the $\widetilde{A}^2A_2$ state.

BIBLIOGRAPHY

[1] T. H. Dunning Jr, *J. Chem. Phys.*, 1989, **90**, 1007–1023.

[2] M. J. Frisch, G. W. Trucks, H. B. Schlegel, G. E. Scuseria, M. A. Robb, J. R. Cheeseman, G. Scalmani, V. Barone, G. A. Petersson, H. Nakatsuji, X. Li, M. Caricato, A. V. Marenich, J. Bloino, B. G. Janesko, R. Gomperts, B. Mennucci, H. P. Hratchian, J. V. Ortiz, A. F. Izmaylov, J. L. Sonnenberg, D. Williams-Young, F. Ding, F. Lipparini, F. Egidi, J. Goings, B. Peng, A. Petrone, T. Henderson, D. Ranasinghe, V. G. Zakrzewski, J. Gao, N. Rega, G. Zheng, W. Liang, M. Hada, M. Ehara, K. Toyota, R. Fukuda, J. Hasegawa, M. Ishida, T. Nakajima, Y. Honda, O. Kitao, H. Nakai, T. Vreven, K. Throssell, J. A. Montgomery, Jr., J. E. Peralta, F. Ogliaro, M. J. Bearpark, J. J. Heyd, E. N. Brothers, K. N. Kudin, V. N. Staroverov, T. A. Keith, R. Kobayashi, J. Normand, K. Raghavachari, A. P. Rendell, J. C. Burant, S. S. Iyengar, J. Tomasi, M. Cossi, J. M. Millam, M. Klene, C. Adamo, R. Cammi, J. W. Ochterski, R. L. Martin, K. Morokuma, O. Farkas, J. B. Foresman and D. J. Fox, *Gaussian˜16 Revision B.01*, 2016, Gaussian Inc. Wallingford CT.

[3] K. Andersson, P. A. Malmqvist, B. O. Roos, A. J. Sadlej and K. Wolinski, *Journal of Physical Chemistry*, 1990, **94**, 5483–5488.

[4] K. Andersson, P. Malmqvist and B. O. Roos, *J. Chem. Phys.*, 1992, **96**, 1218–1226.

[5] R. Sarkar, P.-F. Loos, M. Boggio-Pasqua and D. Jacquemin, *J. Chem. Theory Comput.*, 2022, **18**, 2418–2436.

[6] B. Römer, G. A. Janaway and J. I. Brauman, *J. Am. Chem. Soc.*, 1997, **119**, 2249–2254.

[7] J. B. Kim, M. L. Weichman, T. I. Yacovitch, C. Shih and D. M. Neumark, *J. Chem. Phys.*, 2013, **139**, 104301.

[8] H.-J. Werner, P. J. Knowles, G. Knizia, F. R. Manby and M. Schütz, *WIREs Computational Molecular Science*, 2012, **2**, 242–253.

[9] V. S. Reddy, S. Ghanta and S. Mahapatra, *Phys. Rev. Lett.*, 2010, **104**, 111102.

[10] S. Ghanta, V. S. Reddy and S. Mahapatra, *Phys. Chem. Chem. Phys.*, 2011, **13**, 14531–14541.

[11] S. N. Reddy and S. Mahapatra, *J. Phys. Chem. A.*, 2013, **117**, 8737–8749.

[12] F. Santoro, R. Improta, A. Lami, J. Bloino and V. Barone, *J. Chem. Phys.*, 2007, **126**, 084509.

[13] F. Santoro, A. Lami, R. Improta, J. Bloino and V. Barone, *J. Chem. Phys.*, 2008, **128**, 224311.

[14] V. Barone, J. Bloino, M. Biczysko and F. Santoro, *J. Chem Theory. Comput.*, 2009, **5**, 540–554.

[15] F. Aleotti, D. Aranda, M. Yaghoubi Jouybari, M. Garavelli, A. Nenov and F. Santoro, *J. Chem. Phys.*, 2021, **154**, 104106.

[16] Y. Liu, D. Aranda and F. Santoro, *Phys. Chem. Chem. Phys.*, 2021, **23**, 16551–16563.

[17] H. Köppel, W. Domcke and L. Cederbaum, *Adv. Chem. Phys.*, 1984, **57**, 140.

[18] T. Pacher, L. Cederbaum and H. Köppel, *J. Chem. Phys.*, 1988, **89**, 7367–7381.

[19] W. Domcke, D. Yarkony and H. Köppel, *Conical intersections: electronic structure, dynamics & spectroscopy*, World Scientific, 2004, vol. 15.

[20] L. Cederbaum, W. Domcke and H. Köppel, *Chem. Phys.*, 1978, **33**, 319–326.

[21] S. Mahapatra, *Accounts of chemical research*, 2009, **42**, 1004–1015.

[22] W. Domcke, H. Köppel and L. Cederbaum, *Mol. Phys.*, 1981, **43**, 851–875.

[23] E. Haller, H. Köppel, L. Cederbaum, G. Bieri and W. Von Niessen, *Chem. Phys Lett.*, 1982, **85**, 12–16.

[24] U. Manthe, *J. Chem. Phys.*, 2015, **142**, 244109.

[25] H.-D. Meyer and G. A. Worth, *Theoretical Chemistry Accounts*, 2003, **109**, 251–267.

[26] G. A. Worth, M. H. Beck, A. Jäckle and H.-D. Meyer, The MCTDH Package, Version 8.2, (2000). H.-D. Meyer, Version 8.3 (2002), Version 8.4 (2007). Current version: 8.4.23 (May 2022). See http://mctdh.uni-hd.de.

[27] L. J. Doriol, F. Gatti, C. Iung and H.-D. Meyer, *J. Chem. Phys.*, 2008, **129**, 224109.

[28] H.-D. Meyer, Journal of Physics: Conference Series, 2005, p. 009.

[29] P. A. M. Dirac, *Proceedings of the Royal Society of London. Series A, Containing Papers of a Mathematical and Physical Character*, 1931, **133**, 60–72.

[30] J. Frenkel *et al.*, *Wave mechanics, advanced general theory*, Oxford, 1934, vol. 436.

[31] H. Köppel and W. Domcke, *Encyclopedia of Computational Chemistry*, 2002, **5**, year.

[32] R. Kosloff and H. Tal-Ezer, *Chem. Phys Lett.*, 1986, **127**, 223–230.

[33] H.-D. Meyer, F. Le Quéré, C. Léonard and F. Gatti, *Chem. Phys.*, 2006, **329**, 179–192.